The Conjugate-Gradient Variational Analysis and Initialization Method: An Application to MONEX SOP 2 Data

MOHAN K. RAMAMURTHY

Department of Atmospheric Sciences, University of Illinois at Urbana-Champaign, Urbana, Illinois

I. M. NAVON

Department of Mathematics and Supercomputer Computations Research Institute, Florida State University, Tallahassee, Florida

(Manuscript received 15 July 1991, in final form 24 December 1991)

ABSTRACT

A conjugate-gradient variational blending technique, based on the method of direct minimization, has been developed and applied to the problem of initialization in a limited-area model in the summer monsoon region. The aim is to blend gridded winds from a high-resolution limited-area analysis with a lower-resolution global analysis for use in a limited-area model that uses the global analyses for boundary conditions. The ability of the variational matching approach in successfully blending meteorological analyses of varying resolutions is demonstrated. Reasonable agreement is found between the blended analyses and the imposed weak constraints, together with an adequate rate of convergence in the unconstrained minimization procedure. The technique is tested on the 1979 onset vortex case using data from the FGGE Summer MONEX campaign. The results indicate that the forecasts made from the variationally matched analyses show positive impact and perform better than those from the unblended analyses.

1. Introduction

The use of the calculus of variations to objectively analyze meteorological fields was first suggested by Sasaki (1955, 1958) when he proposed an initialization method that incorporated certain dynamical constraints in the postanalysis adjustment step. In this variational method, one seeks to minimize, in a least-squares sense, the variance of the difference between "observed" and analyzed variables, subject to a set of imposed constraints. Subsequently, Sasaki (1969, 1970a, 1970b) generalized the constrained minimization method to include both strong, as well as weak, constraints and to include time-variation and dynamical constraints so as to filter high-frequency noise from analyses. In Sasaki's terminology, a constraint is defined to be a strong constraint when an equality constraint is identically equal to zero, while a weak constraint is one in which the equality constraint is only approximately equal to zero. The weak-constraint formulation, in fact, can be shown to be equivalent to the first step in a penalty-constrained minimization method. In the traditional variational formulation, a variational functional is first defined, the minimization of which leads to a set of Euler–Lagrange equations, which, in turn, can be expressed as an elliptic partial differential equation and then solved using some iterative numerical technique. During the 1970s and early 1980s, several researchers had applied Sasaki's classical variational approach to different meteorological problems (e.g., Stephens 1970; Lewis 1972; Lewis and Grayson 1972; Sasaki and Goerss 1982; Navon 1981; Navon and de Villiers 1983).

One of the basic purposes of a weak-constraint formulation is to filter and suppress unnecessary high-frequency waves in the initial data while at the same time satisfying certain known dynamical constraints. A major difficulty with the classical variational approach using explicitly derived Euler–Lagrange equations for large-scale (i.e., systems involving a large number of degrees of freedom) meteorological problems, not withstanding its intrinsic complexity, has been the prohibitively expensive computational cost associated with the minimization process, particularly for those problems involving many dynamical constraints. In most cases of real interest, however, this approach has not proven particularly useful or promising since it can lead to partial differential equation systems of mixed type, where considerable numerical and regularity problems arise in all but the simplest cases (Ghil and Malanotte-Rizzoli 1991). In the last several years, however, a new class of variational analysis methods have emerged, those which are better suited for minimization of nonlinear objective func-

Corresponding author address: Prof. I. M. Navon, Florida State University, Department of Mathematics, B-186, Tallahassee, FL 32306-4052.

tions that contain a large number of degrees of freedom (Navon and Legler 1987). These methods range from simple methods such as the steepest-descent method, which exhibits slow, linear convergence, to Newton and quasi-Newton methods, which have quadratic and superlinear rates of convergence, respectively. Unfortunately, Newton methods suffer from a significant computational impediment because they require storage of the Hessian, an $N \times N$ matrix of second derivatives of the objective function containing N degrees of freedom. On the other hand, there exists a class of methods, known as conjugate-gradient (CG) methods, which are iterative descent methods and which produce a better approximation to the local minimum of an objective function with each iteration, that require storage of only a few vectors of length N (e.g., Hoffman 1982, 1984; Testud and Chong 1983; Legler et al. 1989; Atlas et al. 1991). Limited-memory quasi-Newton methods represent a class of algorithms that can be seen as extensions of the CG methods, in which the addition of some modest storage serves to accelerate the convergence rate (Zou et al. 1991).

In this research, we extend the problem of variational analysis using weak constraints to a direct minimization problem, previously proposed by Hoffman (1984), Navon and Legler (1987), and Legler et al. (1989), via the method of conjugate gradients. Their approach is adapted here to an initialization problem to smooth out nonrepresentative, high-frequency meteorological fluctuations in the initial conditions provided to a primitive equation model. The aim is to blend gridded winds from a high-resolution limited-area analysis with a lower-resolution global analysis for use in a limited-area model that uses the global analyses for boundary conditions. Specifically, the technique of direct minimization (see Hoffman 1984; Navon and Legler 1987) is applied here to perform the variational blending.

The variational-blending technique allows information from a myriad of sources to be combined *optimally* by minimizing the lack of fit to information from all those sources while including other suitably defined a priori dynamical constraints. For example, the high-resolution objective analysis obtained over a limited-area domain using the First Global Atmospheric Research Program (GARP) Global Experiment (FGGE) level IIb observations can be reconciled with the European Centre for Medium-Range Weather Forecasts (ECMWF) level IIIb gridded analyses, subject to a set of dynamic constraints imposed on the resultant field. Because the constraints are only "weakly" imposed, they are expected to hold only approximately in the final analysis. In this respect, the variational approach is fundamentally different from a Cressman-type objective analysis approach, where the large-scale information is communicated to the final analysis strictly through the first-guess field, without regard for dynamical constraints. In other words, the resulting analysis does not necessarily have to meet any of the dynamical constraints one might wish to see obeyed. Such dynamical constraints often become important when the analyses are subsequently used in numerical prediction models. On the other hand, if an optimum-interpolation (OI) technique is used to perform the analysis, then it does obviate the need for a subsequent variational-blending step provided the OI technique accounted for the dynamical constraints in the first-guess error covariances and the first-guess field (Phillips 1982). In the mathematical literature, a weak-constraint procedure, such as the one used in this study, is referred to as *unconstrained optimization.* Although the principles underlying the suggested formalisms are similar to previous applications of the calculus of variations to selective matching of meteorological fields (e.g., Stephens 1970; Seaman et al. 1977; Holl et al. 1979), both the methodology adopted here to carry out the direct minimization procedure and the application are quite different. For example, the fields by information blending (FIB) method of Holl et al. consists of a cyclic process of assembly, blending, and data weight reevaluation until the desired degree of accuracy in the final analysis is achieved. The FIB method, as originally proposed by Holl et al. (1979), was developed for a special purpose and was designed to analyze a particular set of variables over a certain domain.

The purpose of this paper is to describe the technique, which, as mentioned above, is based on the CG method for direct minimization, and its application to a specific initialization problem. In particular, the objective of the paper is to demonstrate that the aforementioned direct minimization technique can be successfully applied to variationally blend meteorological analyses, thereby alleviating some of the frequently encountered problems with limited-area high-resolution analyses. For example, a regional analysis, such as the one used in this study, is not obtained using a continuous data-assimilation system. As such, the circulations in the regional domain are not well spun up, which would be the case with the ECMWF gridded fields that are obtained from a four-dimensional data-assimilation system. Moreover, because of the limited extent of the analysis domain, the planetary-scale features are not always accurately portrayed in the regional analysis. Now we present the outline of this paper. In section 2, the overall methodology and the specific application to the problem of variational blending are discussed. A brief description of the CG algorithm is presented in section 3, along with the details of its numerical implementation. We present in section 4 a description of the dataset used in this study and the synoptic overview of the onset vortex case to which the present technique is applied. Section 5 contains the particulars of the numerical prediction model used, along with the description of the experiments. Finally, the results from the application of the variational-blending procedure on the resulting analyses and the subsequent impact on the forecasts of the model are presented in section 6.

2. Variational-blending technique

As mentioned in the Introduction, the primary interest lies in blending a high-resolution analysis performed over a limited domain with a relatively coarse-mesh analysis obtained from the ECMWF global data-assimilation system. The variational blending is confined only to wind data for the following two reasons: (a) it is widely recognized that, due to the barotropic nature of the atmosphere, the temperature variations in the tropics are quite small and are often within the range of measurement errors of the instrument, therefore, the wind field in the tropics is more reliable than the temperature field; (b) geostrophic adjustment theory dictates that the mass field should adjust to the winds in the tropics (e.g., Washington 1964; Williamson and Dickinson 1972). As a result of the breakdown of the geostrophic balance in the tropics, wind observations are particularly important from the standpoint of numerical weather prediction. Moreover, given the importance of organized convection in the tropical circulation, it is even more important to obtain reliable estimates of the divergent component of the wind. The variational matching of winds is accomplished using the CG unconstrained minimization technique, which is described in detail in the following section.

Before the variational matching can be performed, however, some consideration is required in the formulation of the cost function (also known as objective function) that is to be minimized. The variational-blending technique, after all, finds the best fit to various sources of information by minimizing a defined cost function, which is a sum of squares of lacks of fit; and the success of the variational method approach, as well as the rate of convergence of the minimization process, are closely tied to the selection of the individual terms within the cost function and their accompanying weights. First, gradient fields, such as vorticity and divergence, generally exhibit a greater degree of variability at shorter wavelengths than the temperature field or individual wind components. Second, the ECMWF IIIb fields were generated using an adiabatic normal-mode initialization procedure (Bengtsson et al. 1982). As a result, diabatically forced divergent motions due to Hadley and Walker circulations are known to be severely damped in the final IIIb analyses (Puri and Bourke 1982; Krishnamurti et al. 1984). Therefore, in order to alleviate the problems due to adiabatically initialized fields, the cost function includes terms that will constrain the vorticity and divergence of the blended wind field to be closer (fit) to those for the fine-mesh analysis. Using different weights, the option of selectively blending or emphasizing the divergent and rotational components of the wind field is also present, although this was not done in this study. On the other hand, the final analysis is explicitly smoothed by including a Laplacian term that is minimized with respect to the coarse-mesh global analysis. It should be mentioned that, in addition to the explicit smoothing via the Laplacian matching, there is also an implicit filtering built into a direct minimization procedure such as the one used in this study, because the objective function matches finite-difference analogs of first derivatives of two analyses representing different scales of motion. In summary, the underlying idea is to enhance the ECMWF global analysis with our enriched fine-mesh analysis in such a way as to retain the large-scale information from a global data-assimilation system and, at the same time, add detailed information at smaller wavelengths from the fine-mesh analysis within the domain of interest. The cost function F to be minimized can be expressed as

$$
\begin{aligned}
F = {} & \frac{1}{L^2}\rho \sum_x \sum_y \sum_p [(u - u_{\mathrm{FR}})^2 + (v - v_{\mathrm{FR}})^2] \\
& + \frac{1}{L^2}\gamma \sum_x \sum_y \sum_p [(u - u_{\mathrm{EC}})^2 + (v - v_{\mathrm{EC}})^2] \\
& + L^2\Gamma \sum_x \sum_y \sum_p \{[\nabla^2(u - u_{\mathrm{EC}})]^2 \\
& + [\nabla^2(v - v_{\mathrm{EC}})]^2\} \\
& + \beta \sum_x \sum_y \sum_p [\nabla\cdot(\mathbf{V} - \mathbf{V}_{\mathrm{FR}})]^2 \\
& + \alpha \sum_x \sum_y \sum_p [\mathbf{k}\cdot\nabla\times(\mathbf{V} - \mathbf{V}_{\mathrm{FR}})]^2, \quad (1)
\end{aligned}
$$

where the subscripts FR and EC stand for fine-resolution analysis of FGGE level IIb data and ECMWF level IIIb analysis, respectively, u and v are the eastward and northward components of the wind, respectively, while the coefficients ρ, γ, Γ, β, and α are weights that control how closely the direct minimization analysis fits or does not fit each constraint. The scaling parameter L is a convenient length scale that allows the bracketed expressions to be of the same order of magnitude, thus accelerating the convergence rate of the unconstrained minimization procedure.

The next step is the specification of the individual weights in the objective function. Ideally, the individual weights (ρ, γ, Γ, β, and α) should be based on the analysis error estimates at different levels and locations for the two analyses and should have three-dimensional spatial variation, since the ratio of the reliability estimates for the two analyses is, among other things, a function of geographical distribution of observations and historical performance of the two models over that region. Several other techniques have also been proposed in the literature to select the choice of weight matrices (e.g., Wahba and Wendelberger 1980). In this study, the weights are prescribed to be uniform over the three spatial directions. Perhaps it is worth mentioning that it is also possible to combine this variational technique with Errico's scale-selection Fourier

filtering approach (Errico 1985, 1987) to selectively blend information on certain wavelengths.

3. The conjugate-gradient method

As the model domain is a rectangular latitude–longitude grid with ten discrete vertical levels and a (46 × 46) horizontal mesh domain, the discrete unconstrained minimization functional contains 46 × 46 × 10 × 2 (or 42 320) components. Essentially, the problem is one of finding a minimum of Eq. (1) in a multidimensional vector space containing 42 320 degrees of freedom. It is easily seen that a problem of this complexity spanning so many manifolds easily qualifies as a large-scale, unconstrained, optimization problem.

Given the computational intensiveness of the problem, a Beale-restarted quasi-Newton, memoryless CG minimization algorithm, CONMIN, was chosen, which is based on a variation of the Shanno (1978a,b) method implemented algorithmically by Shanno and Phua (1980). The CONMIN routine is available from ACM Algorithms Distribution Service. A description of the Shanno–Phua algorithm follows.

Step (i): Choosing the vector. Let $\mathbf{x}_0$ be the vector

$$\mathbf{x}_0 = (u_{111} \cdots, u_{N_xN_yN_p}, v_{111} \cdots, v_{N_xN_yN_p})^{\mathrm{T}}$$

for the three-dimensional limited-area domain in x, y, and p, where $N_x\Delta_x = L$, $N_y\Delta_y = D$, and $N_p\Delta_p = H$. The initial estimate of the Hessian matrix of second derivatives $\mathbf{H}_0 = \mathbf{I}$, and

$$f_k = f(x_k)$$

is computed using the functional in (1) as well as $g_k = \nabla f(x_k)$, the gradient of g, $s_k = -g_k$, the first CG direction, and

$$s_k^T g_{k+1} = 0.$$

Step (ii): Linear step-size search. Then a linear search is performed to find an optimum step length α_k satisfying the following two conditions:

$$f(x_k + \alpha_k s_k) < f(x_k) + 0.00001\alpha_k s_k^T g_k$$

$$|s_k^T g(x_k + \alpha_k s_k) s_k^T g_k| < 0.9.$$

Step (iii): Test for convergence. Set

$$x_{k+1} = x_k + \alpha_k s_k$$

$$f_{k+1} = f(x_{k+1})$$

$$g_{k+1} = g(x_{k+1})$$

$$p_k = x_{k+1} - x_k$$

$$y_k = g_{k+1} - g_k.$$

If $|g_{k+1}| \leqslant \epsilon \max(1, \|x_{k+1}\|)$, then stop. If not, proceed to step (iv), where ϵ is a predetermined tolerance.

Step (iv): Beale restart. Perform a Beale (1972) restart procedure according to the Powell (1977) criteria; namely, (a) the iteration of k is a multiple of n, the number of variables in the function to be minimized, or (b) $|g_{k+1}^T g_k| \geqslant \|g_{k+1}\|^2$.

If either of the two conditions holds, compute the new search direction s_{k+1} by

$$s_{k+1} = \gamma g_{k+1} - \left[\left(1 + \frac{\gamma y_k^T y_k}{p_k^T y_k}\right)\frac{p_k^T g_{k+1}}{p_k^T y_k} - \frac{\gamma y_k^T g_{k+1}}{p_k^T y_k}\right] + \frac{\gamma p_k^T g_{k+1}}{p_k^T y_k} y_k,$$

where $\gamma = p_k^T y_k / y_k^T y_k$.

Set $p_t = s_k$ and $y_t = y_k$ and go to step (ii), the linear search procedure.

Step (v): Two-step memoryless BFGS scheme. Compute the new search direction by a two-step memoryless BFGS scheme as suggested by Shanno (1978a,b). That is, compute s_{k+1}, the new search direction, by

$$s_{k+1} = -\hat{H}_k g_{k+1} + \frac{p_k^T g_{k+1}}{p_k^T y_k}\hat{H} y_k - \left[\left(1 + \frac{y_k^T \hat{H}_k y_k}{p_k^T y_k}\right)\frac{p_k^T g_{k+1}}{p_k^T y_k} - \frac{y_k^T \hat{H}_k g_{k+1}}{p_k^T y_k}\right] p_k.$$

Here $\hat{H}$ is an approximation to the inverse Hessian, while the vector $\hat{H}_k g_{k+1}$ and $\hat{H}_k y_k$ are defined by

$$\hat{H}_k g_{k+1} = \frac{p_t^T y_t}{y_t^T y_t} g_{k+1} - \frac{p_k^T g_{k+1}}{y_t^T y_t} y_t + \left(\frac{p_t^T g_{k+1}}{p_t^T y_t} - \frac{y_t g_{k+1}}{y_t^T y_t}\right) p_t$$

and

$$\hat{H}_k y_k = \frac{p_t^T y_t}{y_t^T y_t} y_k - \frac{p_t^T y_k}{y_t^T y_t} y_t + \left(2\frac{p_t^T y_k}{p_t^T y_t} - \frac{y_t y_k}{y_t^T y_t}\right) p_t.$$

As suggested by Fletcher (1972), the search direction vector $\mathbf{s}_{k+1}$ is scaled by

$$\hat{f}_{k+1} = [2(f_{k+1} - f_k)/g_{k+1}^T s_{k+1}] s_{k+1}.$$

The scaling is used only for each nonrestart step.

Go to step (ii).

The CG algorithm used in the present study is an optimized version of CONMIN (Shanno and Phua 1980) and forms the basis of current quasi-Newton–like limited-memory methods, such as the variable storage method of Buckley and Lenir (1983, 1985) and Buckley (1989) and the E04DGF algorithm (Gill and Murray 1979) of the Numerical Algorithm Group (NAG) library (1987, Mark 12 Update). As is well known (see Navon and Legler 1987) for solving large-scale nonlinear optimization problems, memory and computational efficiency considerations mandate the

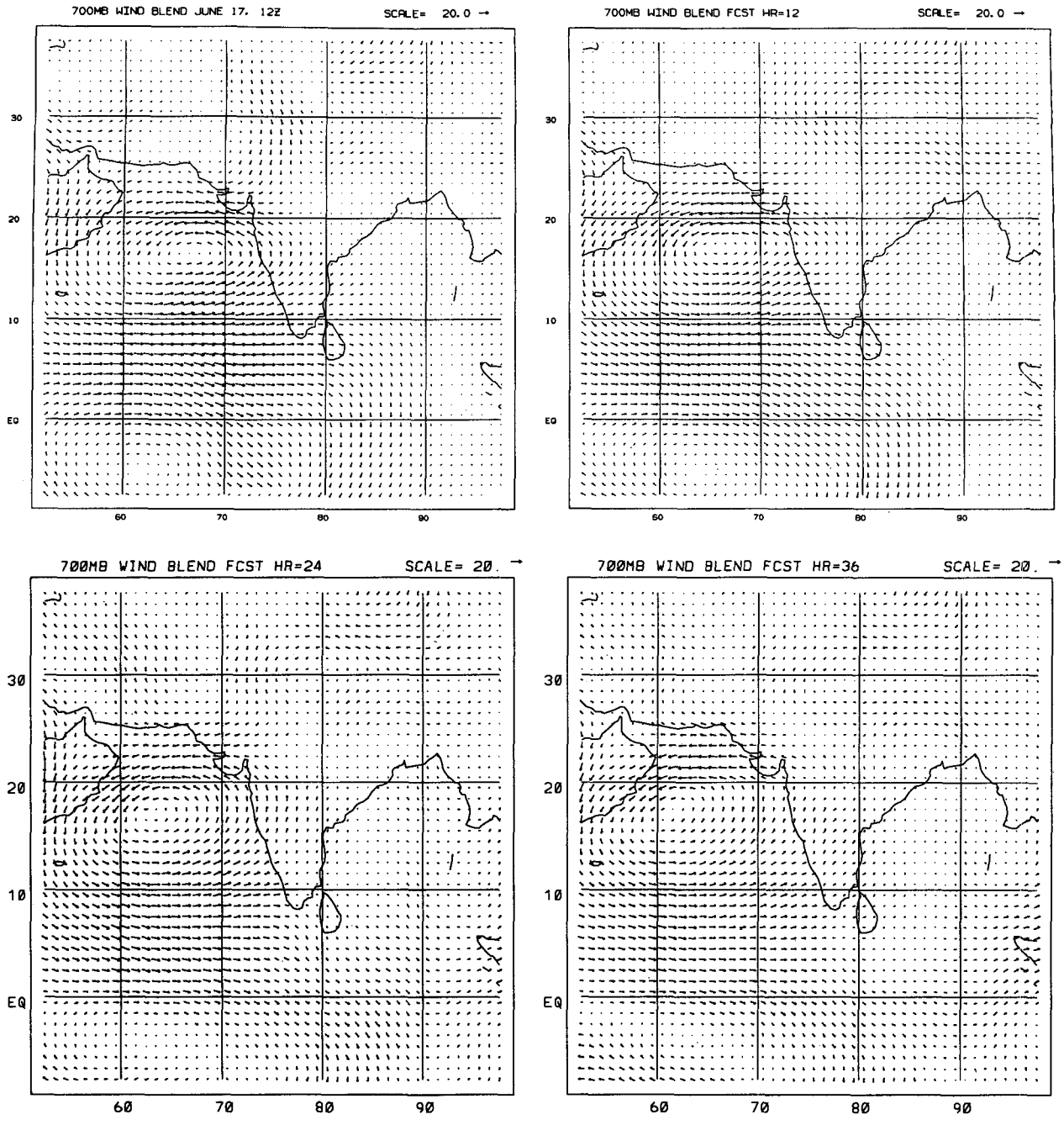

FIG. 1. (a) The 700-mb wind field for the variationally blended initial state valid at 1200 UTC 17 June 1979; (b) 12-h forecast from (a); (c) 24-h forecast; (d) 36-h forecast.

use of CG-type algorithms. In fact, Derber (1985, 1987) has successfully applied a similar technique to the problem of variational four-dimensional analysis using quasigeostrophic constraints. The CONMIN CG algorithm was recently revised for efficient vectorization by Navon et al. (1988, 1990). The vectorized version resulted in a significant speedup on a CYBER-205 supercomputer for the given, as well as other, large-scale nonlinear optimization problems. Recently, Liu and Nocedal (1989) and Gilbert and Lemarechal (1989) have proposed a more efficient variable-storage, limited-memory, quasi-Newton method (L-BFGS). This method has been tested recently by Navon et al. (1991) on a four-dimensional data-assimilation application to an adiabatic version of the National Meteorological Center spectral model and was found to be efficient

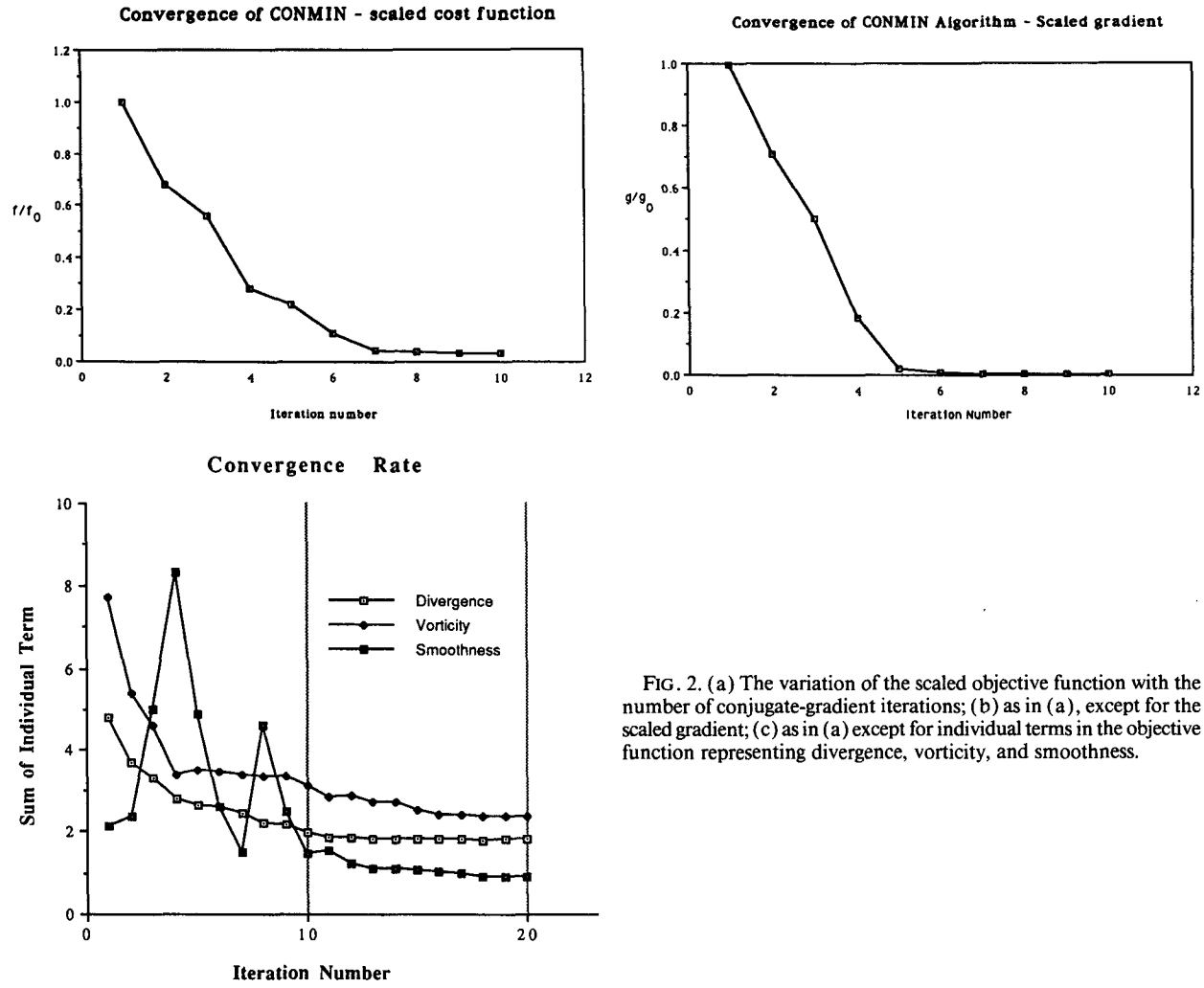

FIG. 2. (a) The variation of the scaled objective function with the number of conjugate-gradient iterations; (b) as in (a), except for the scaled gradient; (c) as in (a) except for individual terms in the objective function representing divergence, vorticity, and smoothness.

and robust in a variety of test problems (Zou et al. 1992).

4. Synoptic overview and dataset

a. Synoptic overview

The variational blending technique proposed here was applied to the Summer Monsoon Experiment (SMONEX) special observing period (SOP 2) dataset. The SMONEX, a regional campaign within FGGE, resulted in an unprecedented data collection over the summer monsoon region, an area that traditionally suffers from paucity of data for numerical weather prediction. Besides the conventional observing network, the SMONEX dataset includes data from several special observing platforms like dropwindsonde observations, satellite cloud-drift winds, constant-level balloon data, and flight-level data from research and commercial aircraft. The particular event for which the analyses are performed in this study is the so-called onset-vortex case of June 1979. During this period (SOP 2) a unique opportunity arose to observe an intense tropical storm over the Arabian Sea, one which was responsible for the onset of the monsoon over the Indian subcontinent. During the second week of June, the Somali jet rapidly intensified, and the resulting barotropic instability of the jet is believed to be responsible for the genesis of a depression in the Arabian Sea on 12 June 1979 (Krishnamurti et al. 1981) just off the west coast of India. In the next several days, the depression intensified rapidly and moved initially northward, in the process establishing the onset of a monsoon over the Indian peninsula. The vortex, which subsequently was classified as a cyclonic storm, with winds in excess of 50 kt in its southern flank, then drifted west-northwestward, eventually making landfall near Oman on 20 June. The 700-mb flow field from the blended (BL) analysis and forecasts, depicting the location and intensity of the onset vortex at 12-h intervals between 1200 UTC 17 June and 0000 UTC 19 June, is shown Figs. 1a–d. A more detailed account of the synoptic situation can

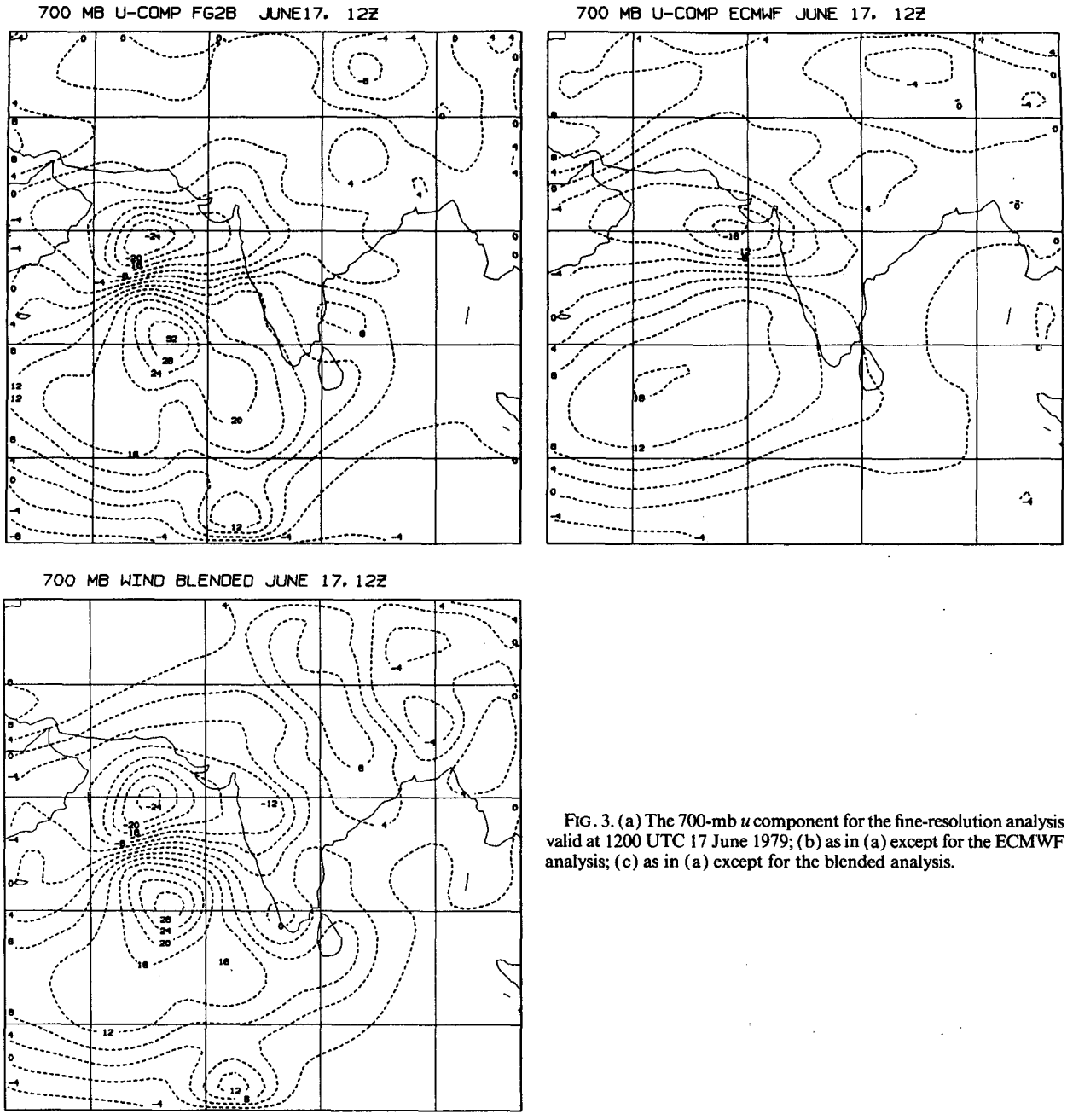

FIG. 3. (a) The 700-mb u component for the fine-resolution analysis valid at 1200 UTC 17 June 1979; (b) as in (a) except for the ECMWF analysis; (c) as in (a) except for the blended analysis.

be found in Krishnamurti et al. (1979) and Ramamurthy and Carr (1987). The various dynamical instabilities associated with this vortex have been examined by Krishnamurti et al. (1981), Mak and Kao (1982), and Mishra et al. (1985). The principal conclusion to be drawn from these studies is that barotropic instability, coupled with latent-heat release due to intense, widespread convection, played a dominant role in the formation and subsequent intensification of the storm, while the direction of movement is largely attributable to the beta effect.

b. Dataset

The significance of the meteorological event, coupled with the richness of the ensuing database, led to the selection of this particular dataset for this study. A multitude of special observations went into the objective analysis phase, including those from dropwindsondes, constant-level balloons, research and commercial aircraft, tropical-wind observing ships, and a satellite. The details of the complete FGGE level IIb dataset used here can be found in Ramamurthy and

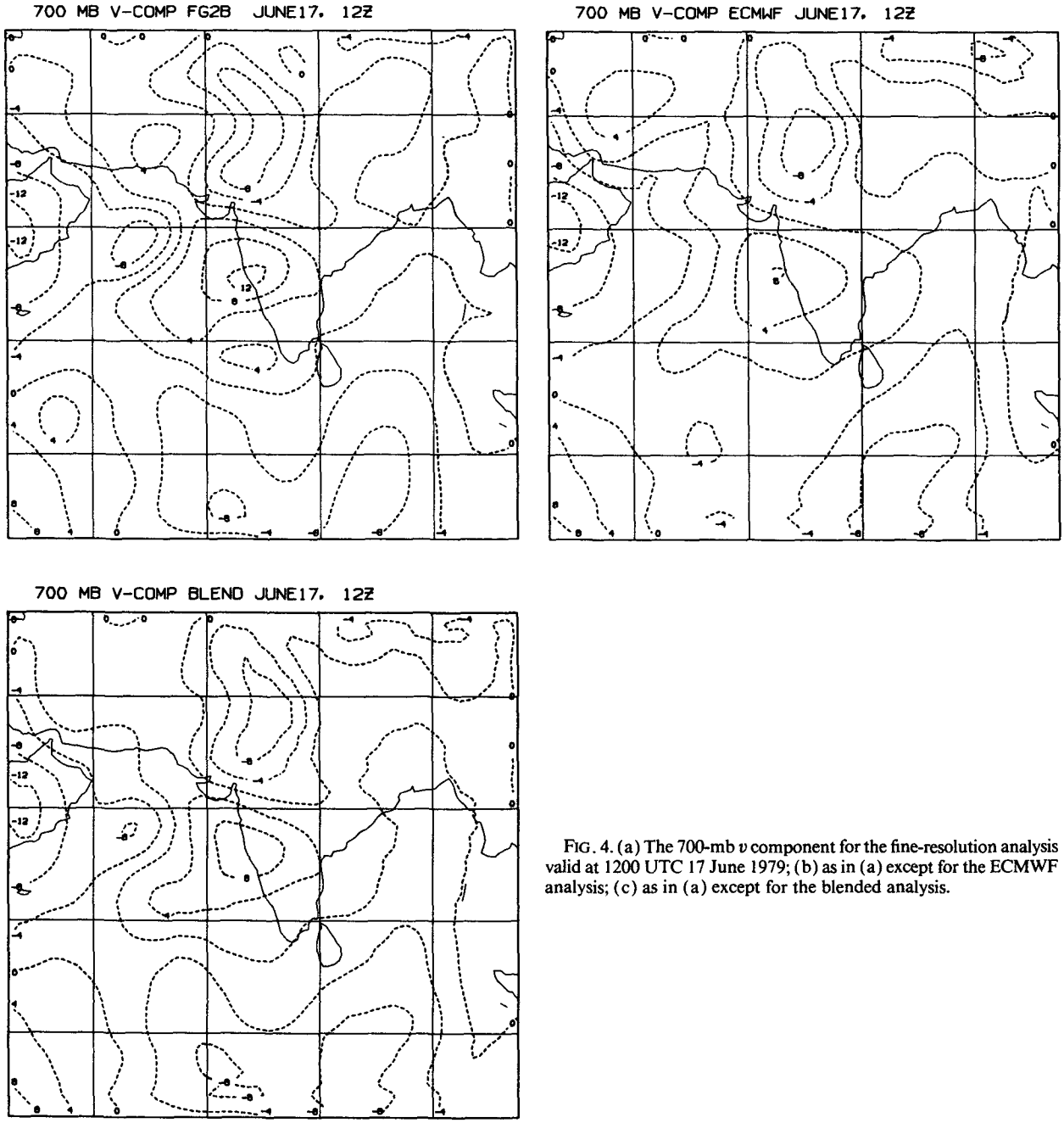

FIG. 4. (a) The 700-mb v component for the fine-resolution analysis valid at 1200 UTC 17 June 1979; (b) as in (a) except for the ECMWF analysis; (c) as in (a) except for the blended analysis.

Carr (1987). To provide the first-guess field for the fine-resolution analysis, the analysis step began with a 12-h integration on a 1° latitude–longitude grid of the forecast model, which is described in the following section. This integration started at 0000 UTC 17 June 1979 and used the FGGE level IIIa analysis, again bilinearly interpolated to a 1° grid. At this time, the onset vortex was near its peak intensity. Using the 12-h forecast values as the first guess, an analysis is performed at 1200 UTC 17 June 1979 of all of the available level IIb observations within a window of ±6 h. The objective analysis scheme is a four-dimensional Cressman (1959) approach, and it uses a Gaussian weighting function in time and logarithmic weights in the vertical direction. To account for the different observational errors associated with the various observing systems, the observations were also weighted for their reliability following Ramamurthy and Carr (1987). Once the fine-resolution analysis is prepared, the resulting wind analyses are variationally blended with the ECMWF

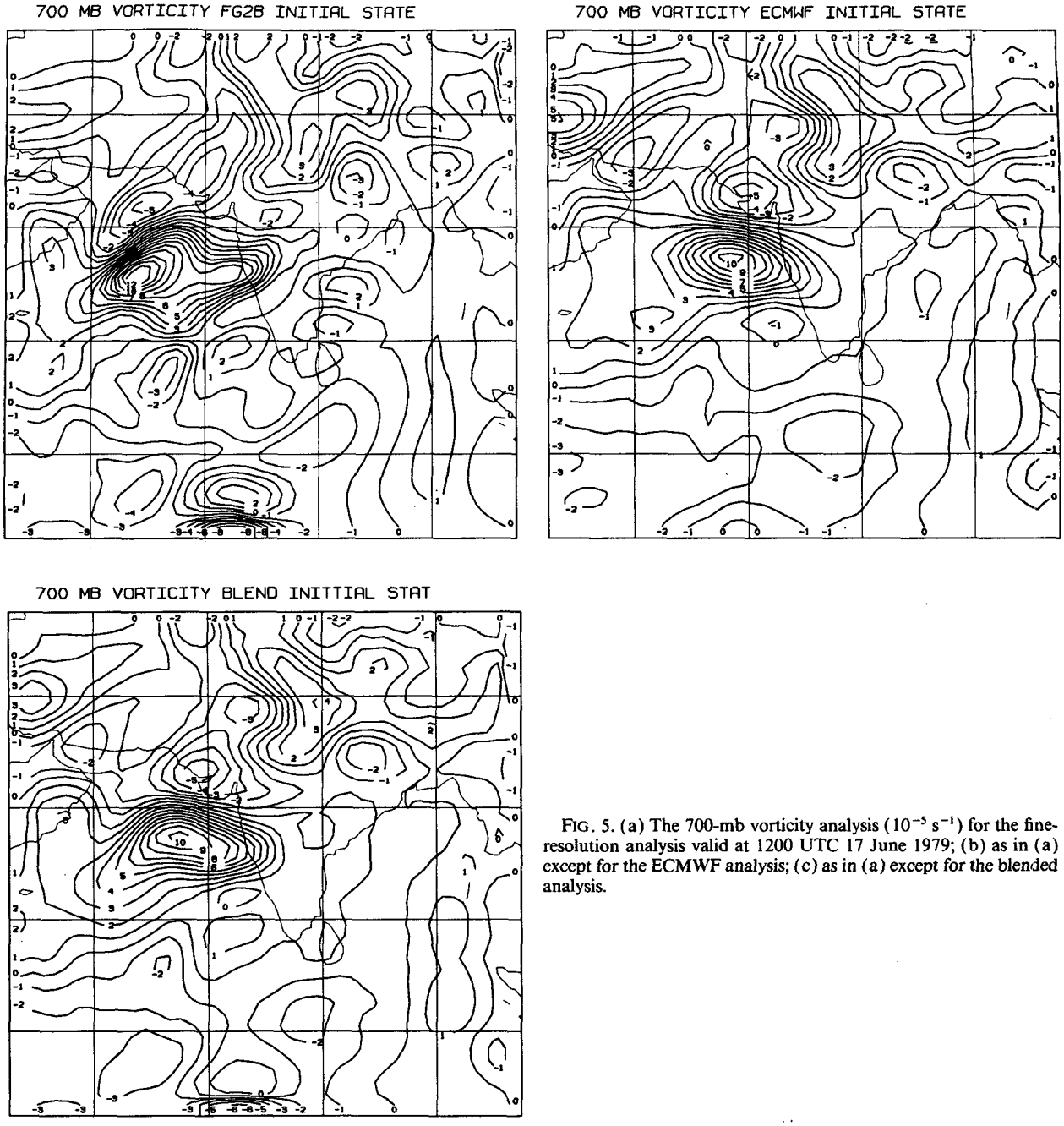

FIG. 5. (a) The 700-mb vorticity analysis (10^{-5} s^{-1}) for the fine-resolution analysis valid at 1200 UTC 17 June 1979; (b) as in (a) except for the ECMWF analysis; (c) as in (a) except for the blended analysis.

level IIIb winds valid at that time, which are also, as before, interpolated bilinearly to a 1° latitude–longitude analysis grid.

5. Model description and experimental design

a. Numerical model

The forecast model used in this study is a pressure-coordinate, limited-area, primitive equation model. There are ten equally spaced (100-mb) levels in the vertical, and the horizontal spacing is 1° × 1° on a latitude–longitude grid. It employs a semi-Lagrangian advection scheme, which is coupled with an Euler-backward scheme for time integration. The model has a fairly complete set of parameterizations for large-scale precipitation, convection, radiation, and boundary-layer physics and is fully described by Ramamurthy (1986) and, to a lesser extent, by Ramamurthy and Carr (1987). The model domain for these experiments extends from 7.5°S to 27.5°N and from 52.5° to

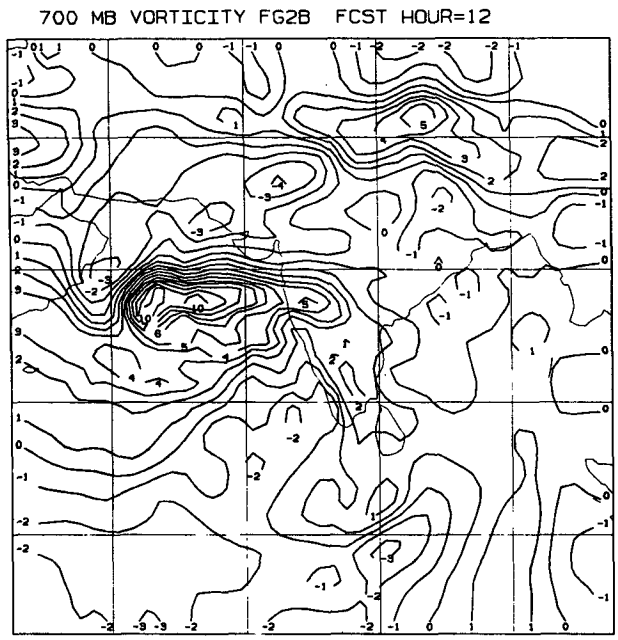

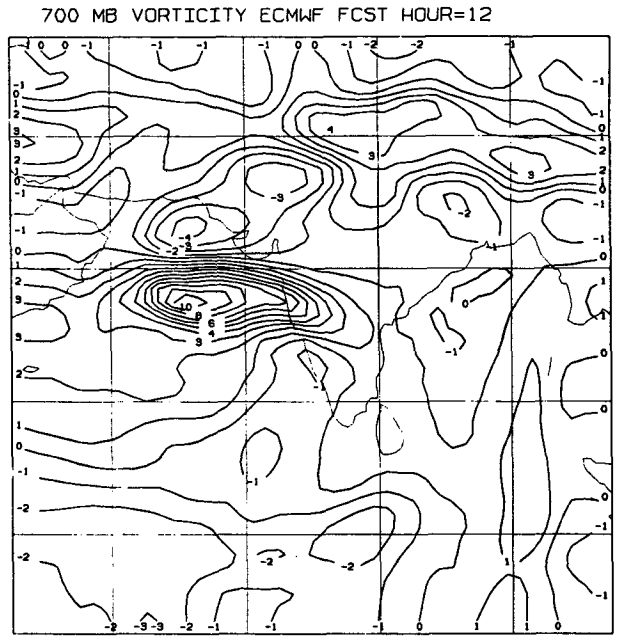

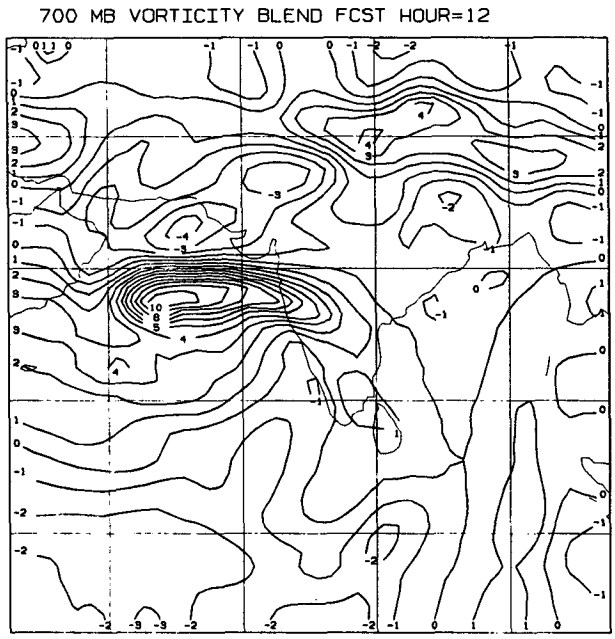

FIG. 6. (a) As in Fig. 5a except for the 12-h forecast; (b) as in Fig. 5b except for the 12-h forecast; (c) as in Fig. 5c except for the 12-h forecast.

97.5°E. Time-varying boundary conditions, derived by interpolating between ECMWF level IIIb analyses at adjacent times, are prescribed along the lateral boundaries via a Perkey–Krietzberg-type scheme (Perkey and Krietzberg 1976).

b. Experiments

Three forecast experiments have been conducted to assess the impact of the aforementioned variational blending approach. The first experiment was performed using only the ECMWF IIIb fields as the initial state at 1200 UTC 17 June 1979. In the second experiment, the initial conditions provided by only the fine-resolution analysis were used. The final experiment has been initialized using the variationally blended fields. All of the initial states are adjusted using the Carr et al. (1983) variational method so as to remove the vertically integrated column divergence. This efficacious procedure helps to eliminate the Lamb wave noise from the initial conditions, while keeping the changes to the analyzed, interpolated, or blended fields to a minimum.

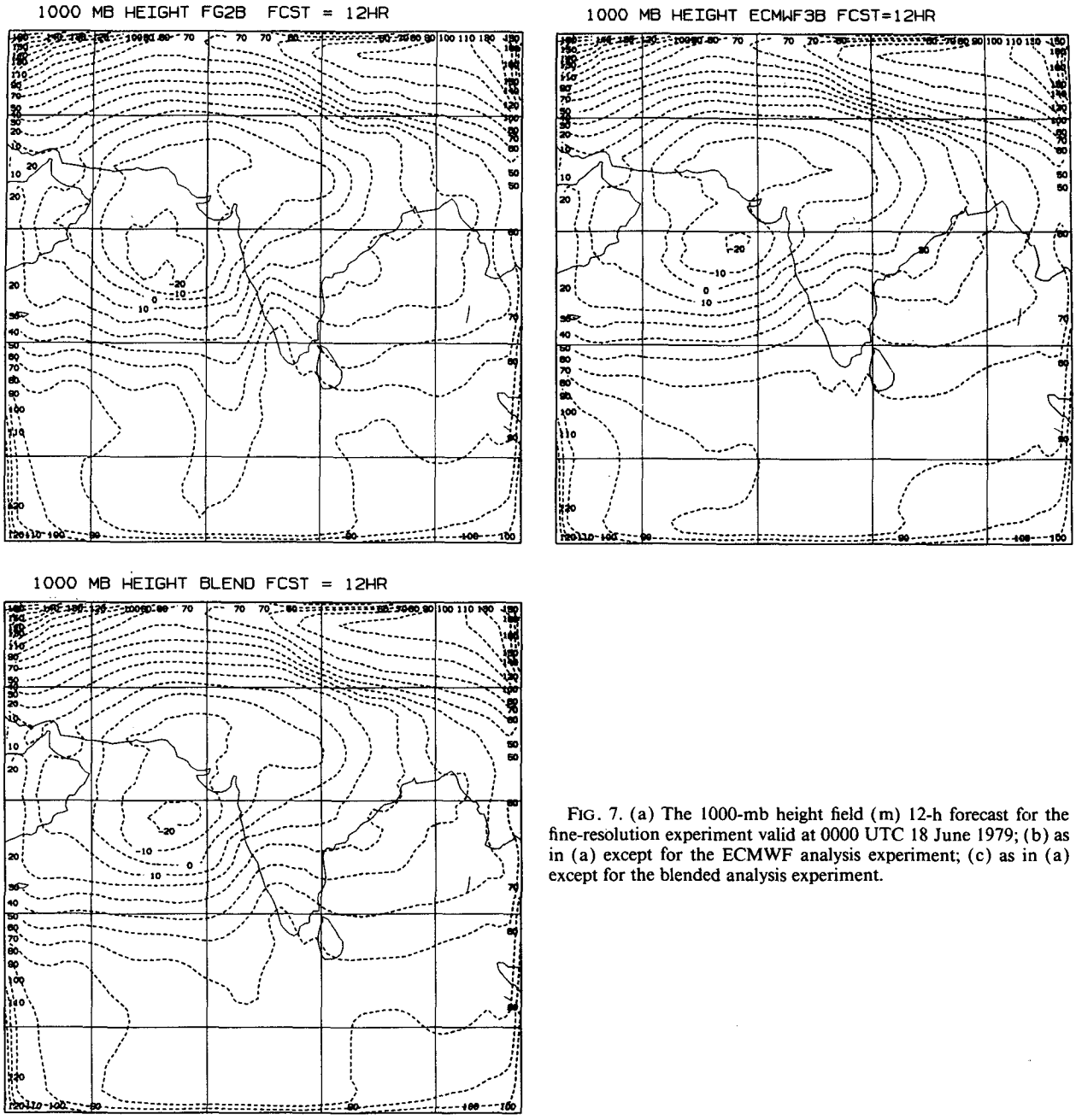

FIG. 7. (a) The 1000-mb height field (m) 12-h forecast for the fine-resolution experiment valid at 0000 UTC 18 June 1979; (b) as in (a) except for the ECMWF analysis experiment; (c) as in (a) except for the blended analysis experiment.

Given the limited size of the model domain used in the experiments and the fact that the impact of the initial state often diminishes rapidly in a regional model after a certain period of time, all forecast integrations are restricted to a period of 24 h from 1200 UTC 17 June 1979.

6. Results and conclusions

We first present the computational results in finding the minimum of the cost function given in (1). Because the CG method requires finding gradient descent (downhill) directions, the minimum found by the CG algorithm could, depending on the convexity of the cost function, the degree of nonlinearity, and the first-guess information provided, be either a local minimum or a global minimum. Despite the large number of variables involved ($n = 42\,320$), the CG algorithm was able to find the minimum of the cost function in about 40 iterations. Like Navon and Legler (1987), we also found that the convergence rate decreased as the minimum was being approached, with CONMIN, the CG

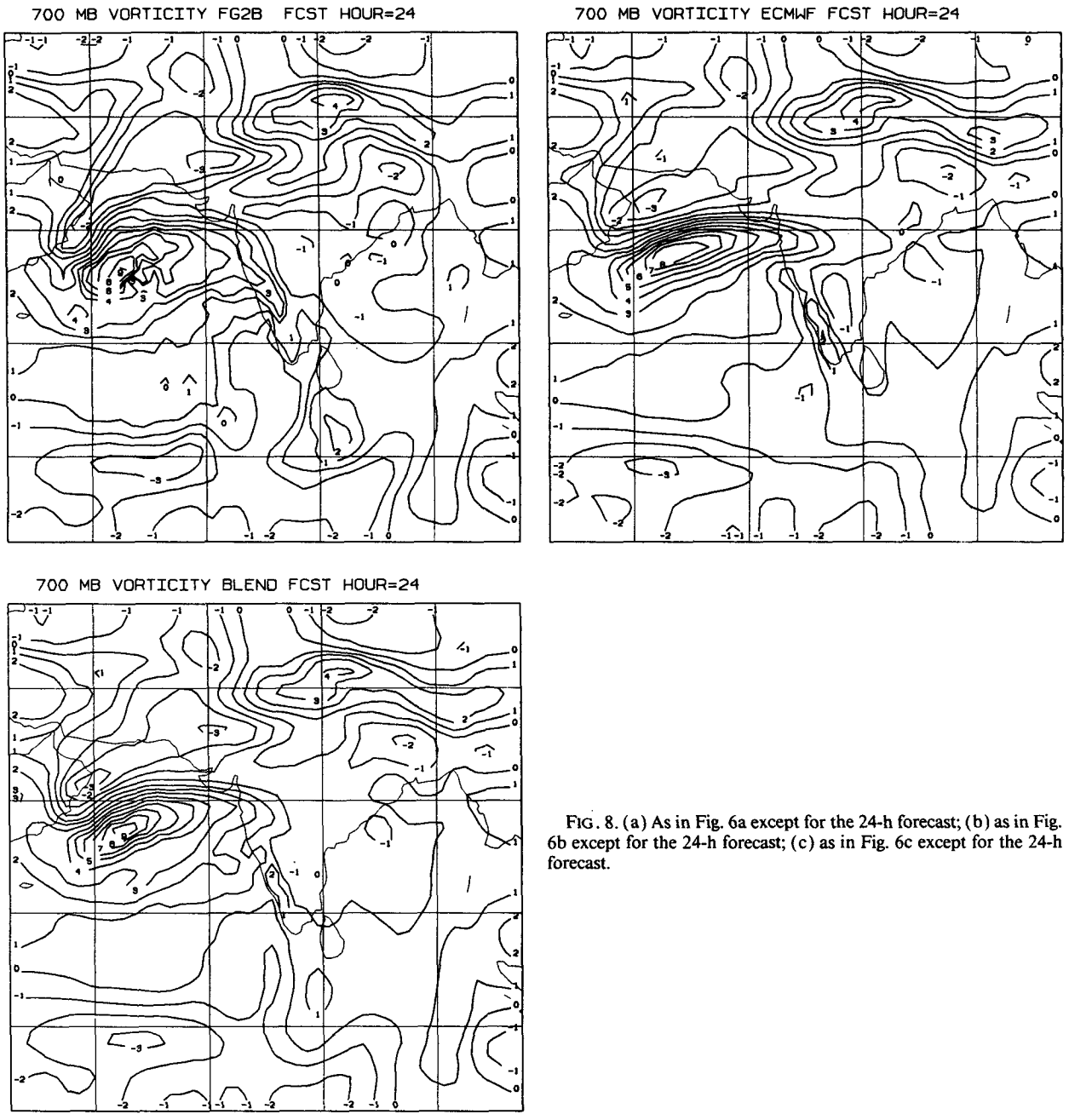

FIG. 8. (a) As in Fig. 6a except for the 24-h forecast; (b) as in Fig. 6b except for the 24-h forecast; (c) as in Fig. 6c except for the 24-h forecast.

algorithm, requiring frequent Beale restarts near the minimum. The behavior of the objective function, scaled by its initial value, is shown in Fig. 2a, while a similar plot for the logarithm of the absolute value of the gradient, also scaled with respect to its initial value of the cost function ($\log_{10}|g/g_0|$), is shown in Fig. 2b. An examination of the convergence rates of the various parts of the cost function are also of some interest, because it would reveal how well the different constraints imposed are evolving during the minimization procedure. The behavior of the individual terms, again scaled with respect to their initial values, as a function of an iteration number is shown in Fig. 2c. It is interesting to note that the vorticity constraint has the steepest convergence rate and is closely followed by the divergence constraint. The Laplacian (smoothness) constraint, on the other hand, wildly oscillates and even initially diverges before slowly exhibiting oscillatory convergence. Given that the case in consideration is an intense tropical storm with a strong rotational component, the faster convergence rate for the vorticity constraint is not entirely surprising. The initial ten-

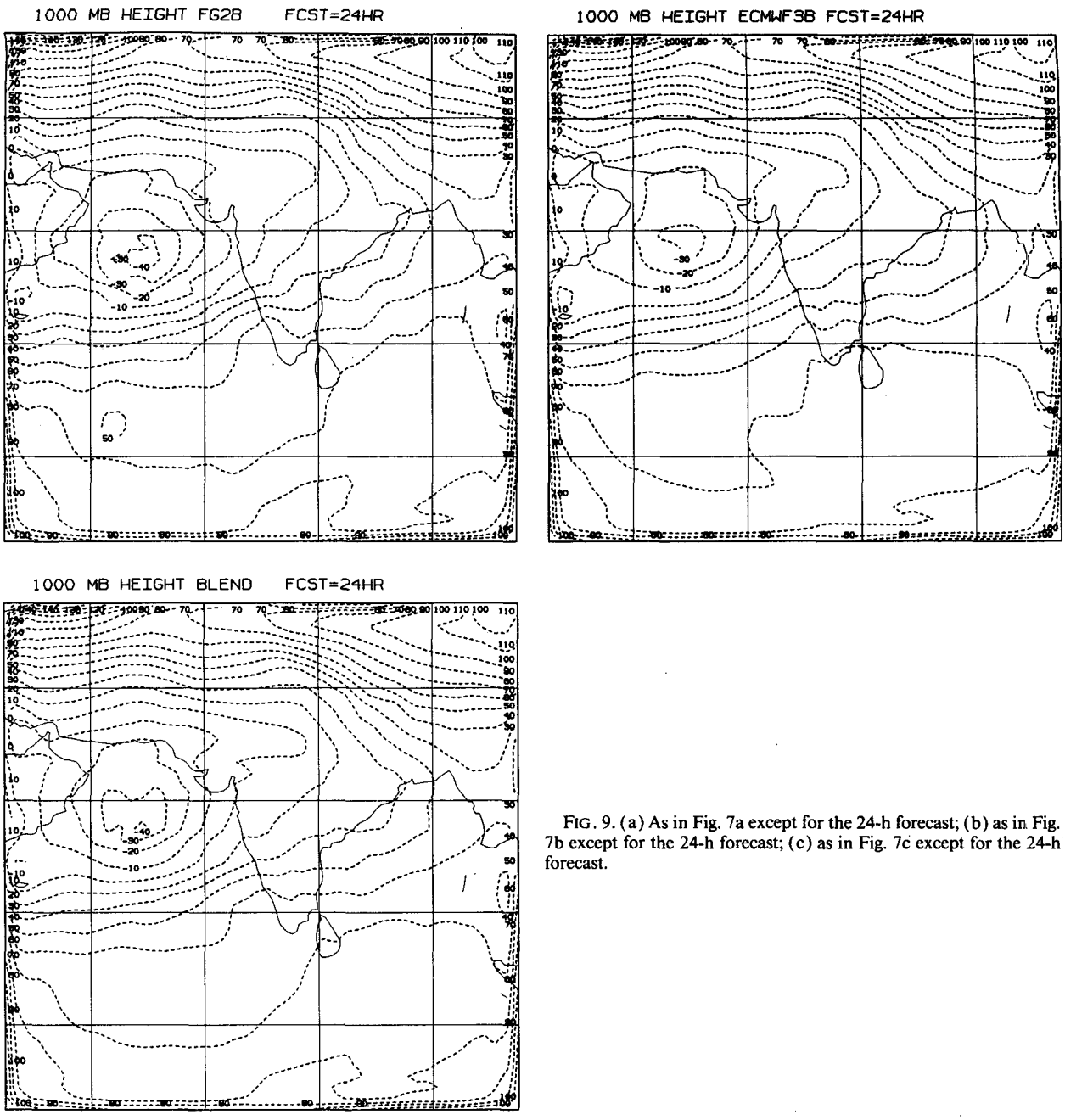

FIG. 9. (a) As in Fig. 7a except for the 24-h forecast; (b) as in Fig. 7b except for the 24-h forecast; (c) as in Fig. 7c except for the 24-h forecast.

dency to diverge in the case of the Laplacian constraint is perhaps due to the fact that there are more constraints in the objective function that are nudging the resulting analysis toward the fine-mesh analysis than there are toward the ECMWF analysis. The examination of the individual terms can also be extended to the selection of weights, thereby providing an inexpensive way to perform sensitivity analysis.

Despite the success of the CG algorithm in this application, a problem that contained a large number of variables, it should be reiterated that other systems may be somewhat less convex or quadratic and, as such, may need a greater number of iterations to converge. In that case, a penalty term containing additional information may have to be included to render the cost function convex. Also, it would be necessary to carefully reformulate the scaling parameter in the cost function so that all of the constraints are of the same order of magnitude, or else the Shanno–Phua conjugate-gradient descent algorithm, with its inexact line searches, will be extremely slow to converge. This, in effect, constitutes a preconditioning approach that

serves two purposes: 1) to reduce the condition number of the Hessian matrix of the cost function, and 2) to cluster its eigenvalues. Another logical extension to the proposed blending method would be the inclusion of spatially inhomogeneous weights that would take into account the density, distribution, and reliability of the observing network. For instance, over data-rich regions there would be more confidence in the analyses, and, correspondingly, a greater weight would be assigned, whereas over data-void regions, the opposite would be the case. It may also be beneficial to increase the weight assigned to the ECMWF analysis along the lateral boundaries, since the first-guess information for the fine-mesh analysis was derived from a limited-area model integration. Nevertheless, based on its overall performance in our application, the CG direct-minimization algorithm shows considerable promise for other large-scale meteorological minimization problems.

The remainder of this section concentrates on the comparison of the variationally blended analysis with those obtained from the ECMWF level IIIb dataset and the fine-resolution regional analysis and also on the impact of the different initial analyses on the ensuing forecasts. In general, the results indicate that the variationally adjusted analysis has succeeded in achieving a reasonable compromise between the ECMWF analysis and our fine-resolution analysis. Figures 3a–c and 4a–c show, respectively, the 700-mb u and v components of the wind field for the three analyses. This level is chosen because 700 mb is near the level of nondivergence for this cyclone and also happens to be the location of strongest vorticity. It is clear from the dipole pattern in, for example, Figs. 3a–c that the strength of the onset vortex is the strongest in the fine-resolution analyses, while the ECMWF analysis portrays a much weaker cyclone. For example, in the southern flank of the onset vortex, the fine-resolution analysis the the westerlies exceed 28 m s^{-1}, while the easterlies, north of the storm, are in excess of 24 m s^{-1}. In comparison, the ECMWF analysis shows a much broader and noticeably weaker region of southwesterly flow equatorward of the vortex. The variationally adjusted analysis, on the other hand, has managed to find a reasonable compromise between these two sets of analyses. The variational matching technique has generated a dipole pattern that is much closer to the fine-resolution analysis than the ECMWF analysis, a consequence of the vorticity constraint term in the objective function. At the same time, the blended analysis, because of the diffusion constraint, has achieved a level of smoothness not evidenced in the fine-mesh analysis. The smoothness of the blended analysis is more readily seen in the gradient quantities, such as divergence and vorticity. Similar features are also noticeable in the 700-mb v fields. In fact, the 700-mb v field for the fine mesh has a well-defined dipole over the Arabian Sea, near the onset-vortex region, while the corresponding v field

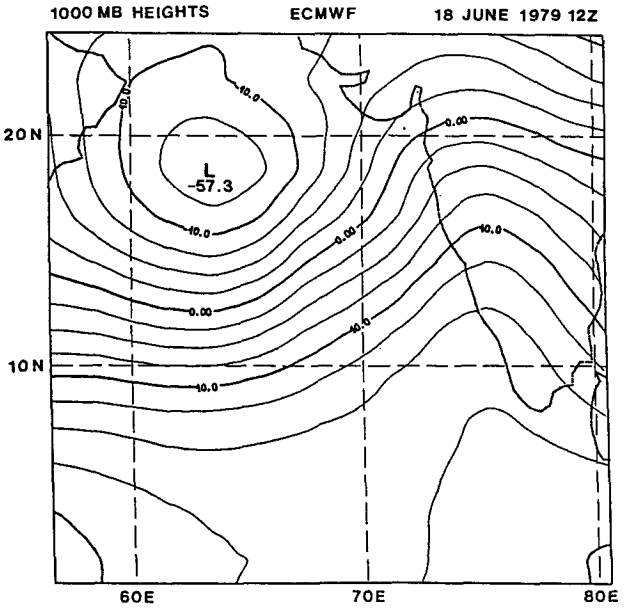

FIG. 10. The 1000-mb height field for the ECMWF analysis valid at 1200 UTC 18 June 1979. This is the verification field for the three 24-h forecasts shown in Fig. 9a–c.

from the IIIb analysis lacks this feature, again indicating a much weaker vortex in the ECMWF global analysis. The vorticity fields for the three analyses are shown in Figs. 5a–c. The BL and EC vorticity fields are smoother than the FR field, whereas the center of the vortex in FR and BL are in closer agreement. Similar results were noticed at other levels near the surface where the vortex was well defined. On the other hand, at higher levels (for example, at 200 mb) the differences between the three analyses were less marked (not shown), since the bulk of the new observations that went into FR were only available at lower levels.

It was noticed that the differences in the forecast fields for the three analyses were consistently smaller than the differences between the respective initial states, particularly with respect to important synoptic features. Given the limited integration domain of the model, the "sweeping out" of forecast differences due to the advection of identical boundary information into the domain from the inflow region is only to be expected (Errico and Baumhefner 1987; Vuckicevic and Errico 1990), leading to the diminishing of the differences between the three forecasts. Plus, the initial state reflects the period when the onset vortex was most intense, subsequent to which the storm weakened in all three integrations, thus diminishing the differences between the three forecasts. For these reasons, our assessment of the forecast impact has been limited to the first 24 h.

A comparison of the 12-h forecasts at the 700-mb level indicates (Figs. 6a–c) that the fine-mesh analysis, albeit somewhat noisier, continues to have the most intense vortex, while the ECMWF forecast has the

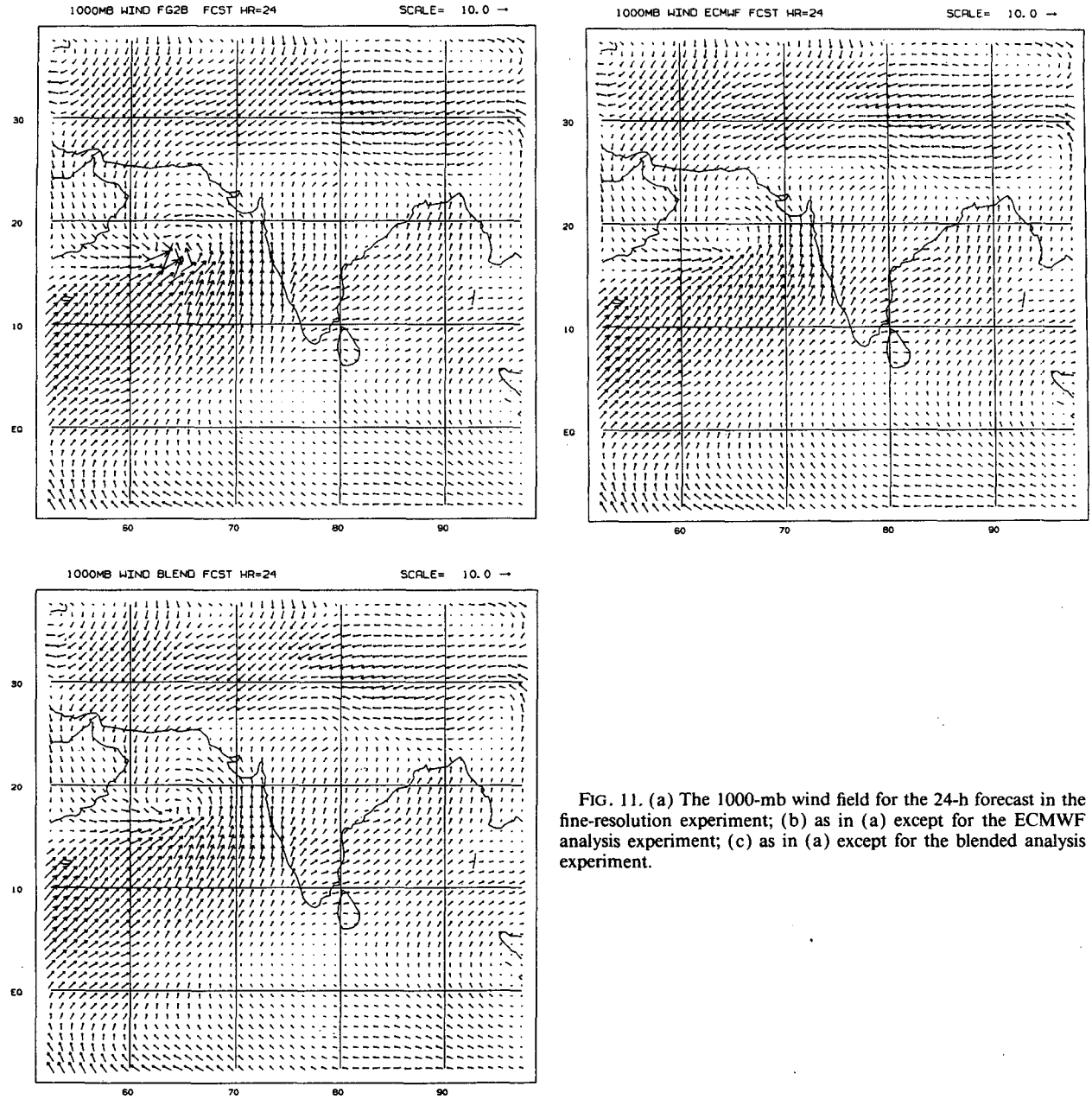

FIG. 11. (a) The 1000-mb wind field for the 24-h forecast in the fine-resolution experiment; (b) as in (a) except for the ECMWF analysis experiment; (c) as in (a) except for the blended analysis experiment.

weakest. As noted earlier, however, the differences are much smaller than those at the initial time. Although the wind field is shown at only one level, similar comparisons were noted at other levels, too. At the surface, that is, the 1000-mb level in this model, the cyclone is once again strongest in the FR forecast and weakest in the EC forecast (Figs. 7a–c). In the next 12 h, forecasts are valid at 1200 UTC 18 June, and shown in Figs. 8a–c and 9a–c, the aforementioned trends continue to prevail, with the forecast from the high-resolution analysis being the most intense as well as the noisiest. The ECMWF verification analysis valid at this time is shown in Fig. 10. Clearly, the low pressure center in the blended forecast is closer to that in the fine-resolution forecast as well as the verification map, but without the embedded noise. Both FR and BL forecasts are approximately 10 m deeper than the EC forecast. Even though the FR forecast depicted the cyclone the strongest, it had the undesirable aspect of being too noisy. This is most evident in the 1000-mb winds, which are shown for the three experiments in Figs. 11a–c. The forecast wind field in the FR experiment is clearly much too noisy compared with that in the BL forecast. In the next 12 h, this noise was found to

TABLE 1. Root-mean-square vector errors (m s^{-1}) for 24-h forecasts over the entire domain.

	ECMWF	FGGE IIb	Blended
1000 mb	6.8	5.9	6.0
700 mb	5.9	5.1	4.9
200 mb	8.1	7.8	7.7

overwhelm the primary circulation around the cyclone in the FR forecast (not shown), indicating the approach of near-blowup conditions in the model. Table 1 shows the root-mean-square (rms) vector errors for the three forecasts valid at 1200 UTC 18 June over the entire model domain. The verification is done against the observations at those levels via bilinear interpolation to observation points. Despite the fact that the differences in the rms errors among the three forecasts are small, the forecast from the variationally blended initial state verifies better than the other two. The positive impact is that the blended analysis becomes more evident when the verification domain is confined to the onset-vortex region, as shown Table 2. The EC forecast is clearly the worst of the three when it comes to statistical verification, whereas the FR forecast has the worst synoptic evaluation. Although these changes are within the variability of the forecasts of this particular model, when random perturbations of similar amplitude are added, the consistent, positive impact of the blended initial state does not seem to be an accident. To test this, experiments were performed by adding random, small-amplitude perturbations to the initial conditions and integrating the model forward. When small-amplitude random perturbations, containing rms differences in the range of 1–1.5 m s^{-1}, were added to the wind-field initial state, the forecasts were consistently and considerably worse than any of the three forecasts shown in this study, confirming the earlier assertion that the improvements afforded by the variational technique, albeit small, were no fluke.

Since one of the positive attributes of the variationally blended fields is its smoothness, we examined how smoothly the model integration starts up with the blended analyses compared with the other two analyses. To this end, we inferred the presence of external inertia–gravity noise by plotting the time history of the vertical motion field at 1000 mb, the lower boundary of the model. The time-series of 1000-mb rms omega,

TABLE 2. Root-mean-square vector errors around onset vortex for 24-h forecasts.

	ECMWF	FGGE IIb	Blended
1000 mb	5.4	5.3	4.2
700 mb	4.7	3.7	3.2
200 mb	6.9	6.4	6.1

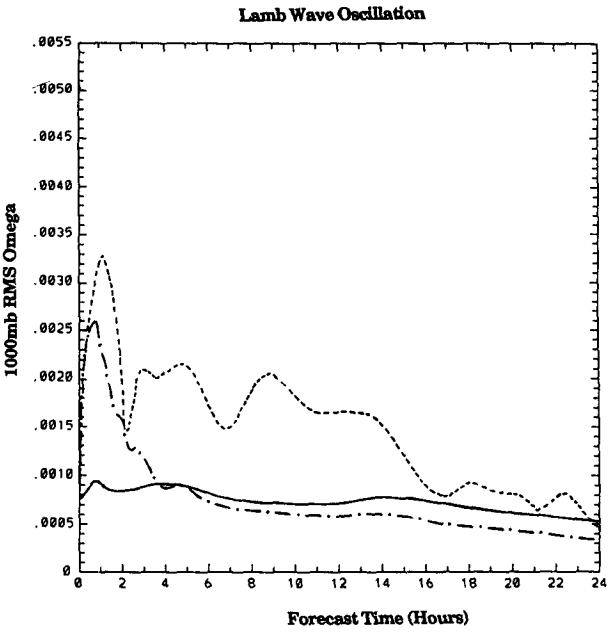

FIG. 12. Root-mean-square vertical velocity (mb s^{-1}) at 1000 mb for the fine-resolution experiment (dashed line), the ECMWF experiment (solid line), and the blended experiment (dash–dot line).

shown in Fig. 12, indicates that both the EC and BL initial states have a smooth evolution after about 3 h, while the high-resolution FR analysis continues to exhibit noisy evolution through the first 16 h. To examine if the noise in the initial conditions affects the spinup period, the time series of the domain-averaged rainfall

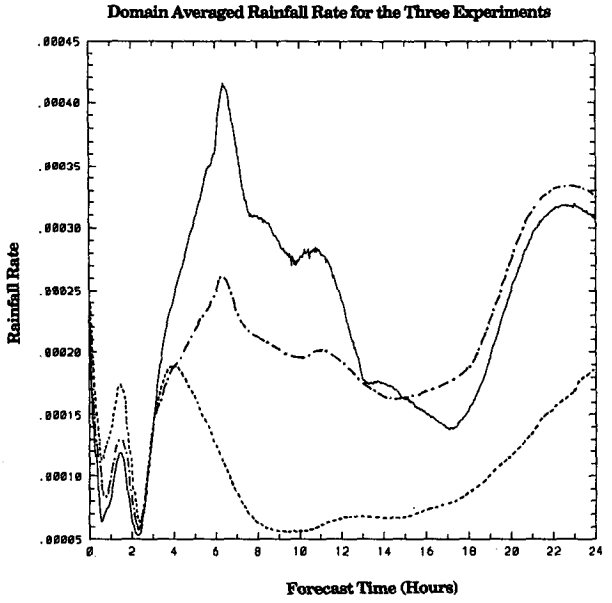

FIG. 13. Domain-averaged rainfall rate (mm s^{-1}) for the fine-resolution experiment (solid line), the ECMWF experiment (small-dash line), and the blended experiment (dash–dot line).

rate for the three experiments is plotted in Fig. 13. It is clear that the EC forecast, which also has the weakest representation of the onset vortex in the initial state, produces the least amount of rain in the first 24 h, whereas FR and BL forecasts show much increased precipitation activity. It is interesting to note that the BL integration, though it starts out with lower precipitation activity than the FR forecast in the first 12 h, leads to greater precipitation rates in the next 12 h. This is an indication of the positive feedback of the rotational modes on precipitation and of a lesser degree of gravity-wave activity in the BL forecasts.

The results presented in this study have shown that the variational blending technique, which is based on a quasi-Newton, memoryless CG minimization algorithm, is readily adaptable to the problem of analysis and initialization of primitive equation models, particularly when presented with analyses of different resolution, data density, and reliability. The ability of the variational CG method to achieve a reasonable compromise between the ECMWF level IIIb global analysis and the much-finer FGGE level IIb analysis has been demonstrated, along with its continued impact in the subsequent forecast stage. The variational low-pass filter built into the cost function via the diffusion (Laplacian) terms has succeeded in suppressing small-scale inconsistencies in the flow patterns. This study has focused on a single application of the CG technique for analysis and initialization. It would be desirable to gauge the success of the method in other synoptic situations using data from other field experiments. Also, for future applications to large-scale minimization problems in meteorology, the CG method should be evaluated for its efficacy and accuracy, along with truncated-Newton methods of Nash and Nocedal (1989) and the BFGS limited-memory method (Liu and Nocedal 1989; Zou et al. 1991), both of which show considerable promise. The sensitivity of the final analysis to the specification of the individual weights for the various constraints in the cost function merits further investigation, too, together with the contribution of the various terms, along the lines of Hall et al. (1982). The problem of variational blending could also be posed as a four-dimensional data-assimilation problem with the same cost functional and data generated by integrating the model using the FR analysis as the initial condition. That would necessitate the derivation of the adjoint model of the present forecast model.

Acknowledgments. We acknowledge the support from the Supercomputer Computations Research Institute (SCRI) at the Florida State University, where the bulk of the computing for this research was performed. SCRI is partially funded by the U.S. Department of Energy through Contract DE-FC05-85ER250000. This research was also supported through National Science Foundation Grants ATM-86-10778 and ATM-88-07128.

REFERENCES

Atlas, R., S. C. Bloom, R. N. Hoffman, J. V. Ardizoone, and G. Brin, 1991: Space-based surface wind vectors to air understanding of air–sea interactions. *Eos Trans.* **72**(18), 201–208.

Beale, E. M. L., 1972: A derivation of conjugate-gradients. *Numerical Methods for Nonlinear Optimization,* F. A. Lootsma, Ed., Academic Press, 39–43.

Bengtsson, L., M. Kanamitsu, P. Kallberg, and S. Uppala, 1982: FGGE 4-dimensional data assimilation at ECMWF. *Bull. Amer. Meteor. Soc.,* **63,** 29–43.

Buckley, A. G., 1989: Remark on Algorithm 630. *ACM Trans. on Math. Software,* **15,** 262–274.

——, and A. Lenir, 1983: QN-like variable storage conjugate gradients. *Math. Program,* **27,** 155–175.

——, and ——, 1985: Algorithm 630-BBVSCG-A variable storage algorithm for function minimization. *Acm. Trans. Math. Software,* **11**(2), 103–119.

Carr, F. H., D. J. Risk, and M. Ramamurthy, 1983: A simple, fast and accurate procedure for initialization of a limited-area model. Preprints, *Sixth Conf. on Numerical Weather Prediction,* Omaha, Nebraska, Amer. Meteor. Soc., 183–187.

Cressman, G. P., 1959: An operational objective analysis system. *Mon. Wea. Rev.,* **94,** 367–374.

Derber, J. C., 1985: The variational 4-D assimilation of analyses using filtered models as constraints. Ph.D. thesis, University of Wisconsin-Madison, 142 pp.

——, 1987: Variational four-dimensional analysis using quasi-geostrophic constraints. *Mon. Wea. Rev.,* **115,** 998–1008.

Errico, R. M., 1985: Spectra computed from a limited-area grid. *Mon. Wea. Rev.,* **113,** 1554–1562.

——, 1987: A comparison between two limited-area spectral analysis schemes. *Mon. Wea. Rev.,* **115,** 2856–2861.

——, and D. P. Baumhefner, 1987: Predictability experiments using a high-resolution limited-area model. *Mon. Wea. Rev.,* **114,** 1625–1641.

Fletcher, R., 1972: *Conjugate Direction Methods for Unconstrained Optimization.* W. Murray, Ed., Academic Press, 144 pp.

Gilbert, J. C., and C. Lemarechal, 1989: Some numerical experiments with variable storage quasi-Newton algorithms. *Math. Programm.,* **45,** 407–435.

Gill, P. E., and W. Murray, 1979: Conjugate-gradient methods for large-scale minimization. Tech. Rep. SOL-79-15. Systems Optimization Laboratory, Department of Operations Research, Stanford, 60 pp.

Ghil, M., and P. Malanotte-Rizzoli, 1991: Data assimilation in meteorology and oceanography. *Advances in Geophysics,* Academic Press, **15,** 262–274.

Hall, M. C. G., D. G. Cacuci, and M. E. Schlesinger, 1982: Sensitivity analysis of a radiative–convective model by the adjoint method. *J. Atmos. Sci.,* **39,** 2038–2050.

Hoffman, R., 1982: SASS wind ambiguity removal by direct minimization. *Mon. Wea. Rev.,* **110,** 434–445.

——, 1984: SASS wind ambiguity removal by direct minimization. Part II: Use of smoothness and dynamical constraints. *Mon. Wea. Rev.,* **112,** 1829–1852.

Holl, M. M., M. J. Cuming, and B. R. Mendenhall, 1979: The expanded ocean thermal-structure analysis system: A development based on the fields by information blending methodology. MII Project, Final Rep. M-241. [NTIS ADA076534.]

Krishnamurti, T. N., P. Ardanuy, Y. Ramanathan, and R. Pasch, 1979: Quick look summer MONEX atlas. Part II. The onset phase. Florida State University Rep. No. 79-5, 312 pp.

——, ——, ——, and ——, 1981: On the onset vortex of the summer monsoon. *Mon. Wea. Rev.,* **109,** 344–363.

——, K. Ingles, S. Cocke, T. Kitade, and R. Pasch, 1984: Details of low latitude medium range numerical weather prediction using a global spectral model. Part II. Effects of orography and physical initialization. *J. Meteor. Soc. Japan,* **62,** 613–649.

Legler, D. M., I. M. Navon, and J. J. O'Brien, 1989: Objective analysis of pseudostress over the Indian Ocean using a direct-minimization approach. *Mon. Wea. Rev.,* **117,** 709–720.

Lewis, J. M., 1972: The operational subsynoptic analysis using the variational method. *Tellus,* **24,** 514–530.

——, and T. H. Grayson, 1972: The adjustment of surface wind and pressure by Sasaki's variational matching technique. *J. Appl. Meteor.,* **11,** 586–597.

Liu, D. C., and J. Nocedal, 1989: On the limited-memory BFGS method for large scale optimization. *Math. Program.,* **45,** 503–528.

Mak, M., and C.-Y. Kao, 1982: An instability study of the onset vortex of the southwest monsoon. *Tellus,* **34,** 358–368.

Mishra, S. K., M. D. Patwardhan, and L. George, 1985: A primitive equation barotropic instability study of the monsoon onset vortex, 1979. *Quart. J. Roy. Meteor. Soc.,* **111,** 427–444.

NAG, 1987: Fortran Library Reference Manual (Mark 12), Numerical Algorithms Group, 3(E04), 1–6, 370 pp. [Available from NAG Limited. Oxford OX7-2DE, England, or NAG INC., Downers Grove, IL 70515.]

Navon, I. M., 1981: Implementation of a posteriori methods for enforcing conservation of potential enstrophy and mass in discretized shallow-water equation models. *Mon. Wea. Rev.,* **109,** 946–958.

——, and R. de Villiers, 1983: Combined penalty multiplier optimization methods to enforce integral invariants conservation. *Mon. Wea. Rev.,* **111,** 1228–1243.

——, and D. Legler, 1987: Conjugate-gradient methods for large-scale minimization in meteorology. *Mon. Wea. Rev.,* **115,** 1479–1502.

——, P. K. H. Phua, and M. K. Ramamurthy, 1988: Vectorization of conjugate-gradient methods for large-scale minimization. *Proc. Supercomputing Conference,* Orlando, The Computer Society of the IEEE, 410–418.

——, ——, and ——, 1990: Vectorization of conjugate-gradient methods for large-scale minimization in meteorology. *J. Opt. Theor. Appl.,* **66,** 71–93.

——, X. Zou, J. Derber, and J. Sela, 1992: Variational data assimilation with an adiabatic version of the NMC spectral model. *Mon. Wea. Rev.,* **120,** 1433–1446.

Nash, S. G., and J. Nocedal, 1989: A numerical study of the limited-memory BFGS method and the truncated-Newton method for large-scale optimization. Tech. Rep., Northwestern University, NAM 02, 19 pp.

Perkey, D. J., and C. W. Kreitzberg, 1976: A time-dependent lateral boundary scheme for limited-area primitive equation models. *Mon. Wea. Rev.,* **104,** 746–755.

Phillips, N. A., 1982: On the completeness of multivariate optimum interpolation for large-scale meteorological analysis. *Mon. Wea. Rev.,* **110,** 1329–1334.

Powell, M. J. D., 1977: Restart procedures for the conjugate-gradient method. *Math. Program,* **12,** 241–254.

Puri, K., and W. Bourke, 1982: A scheme to retain the Hadley circulation during nonlinear normal mode initialization. *Mon. Wea. Rev.,* **110,** 327–335.

Ramamurthy, M. K., 1986: Four-dimensional data assimilation on a limited-area model for the monsoon region. Ph.D. dissertation. The University of Oklahoma, 306 pp.

——, and F. H. Carr, 1987: Four-dimensional data assimilation in the monsoon region. Part I: Experiments with wind data. *Mon. Wea. Rev.,* **115,** 1678–1706.

Sasaki, Y. K., 1955: A fundamental study of the numerical prediction based on the variational principle. *J. Meteor. Soc. Japan,* **33,** 262–275.

——, 1958: An objective analysis based on the variational method. *J. Meteor. Soc. Japan,* **36,** 77–88.

——, 1969: Proposed inclusion of time-variation terms, observational and theoretical, in numerical variational objective analysis. *J. Meteor. Soc. Japan,* **47,** 115–203.

——, 1970a: Some basic formalisms in numerical variational analysis. *Mon. Wea. Rev.,* **98,** 857–883.

——, 1970b: Numerical variational analysis formulated under the constraints as determined by long-wave equations as a low-pass filter. *Mon. Wea. Rev.,* **98,** 884–898.

——, and J. S. Goerss, 1982: Satellite data assimilation using NASA data systems test 6 observations. *Mon. Wea. Rev.,* **110,** 1635–1644.

Seaman, R. S., R. Falconer, and J. Brown, 1977: Application of a variational blending technique to numerical analysis in the Australian region. *Austr. Meteor. Mag.,* **25,** 1–22.

Shanno, D. F., 1978a: Conjugate-gradient methods with inexact searches. *Math. Oper. Research,* **3,** 244–256.

——, 1978b: On the convergence of a new conjugate-gradient method. *SIAM Jour. Numer. Anal.,* **15,** 1247–1257.

——, and K. H. Phua, 1980: Remark on algorithm 500. *ACM Trans. Math. Software,* **6**(4), 618–622.

Stephens, J. J., 1970: Variational initialization with the balance equation. *J. Appl. Meteor.,* **9,** 732–739.

Testud, J., and M. Chong, 1983: Three-dimensional wind field analysis from dual-Doppler radar data. Part I: Filtering, Interpolating and differentiating the raw data. *J. Climate Appl. Meteor.,* **22,** 1204–1215.

Vukicevic, T., and R. M. Errico, 1990: The influence of artificial and physical factors upon predictability estimates using a complex limited-area model. *Mon. Wea. Rev.,* **118,** 1460–1482.

Wahba, G., and J. Wendelberger, 1980: Some new mathematical methods for variational objective analysis using splines and cross-validation. *Mon. Wea. Rev.,* **108,** 1122–1143.

Washington, W. M., 1964: A note on the adjustment towards geostrophic equilibrium in a simple fluid system. *Tellus,* **16,** 530–534.

Williamson, D. L., and R. E. Dickinson, 1972: Periodic updating of meteorological variables. *J. Atmos. Sci.,* **29,** 190–193.

Zou, X., I. M. Navon, M. Berger, M. K. Phua, T. Schlick, and F. X. LeDimet, 1992: Numerical Experience with limited-memory, quasi-Newton methods for large-scale unconstrained nonlinear minimization. *SIAM J. Optimization,* in press.